JACS
JOURNAL OF THE AMERICAN CHEMICAL SOCIETY
pubs.acs.org/JACS
Communication

A Curved Graphene Nanoribbon with Multi-Edge Structure and High Intrinsic Charge Carrier Mobility

Wenhui Niu, Ji Ma, Paniz Soltani, Wenhao Zheng, Fupin Liu, Alexey A. Popov, Jan J. Weigand, Hartmut Komber, Emanuele Poliani, Cinzia Casiraghi, Jörn Droste, Michael Ryan Hansen, Silvio Osella, David Beljonne, Mischa Bonn, Hai I. Wang, Xinliang Feng, Junzhi Liu,* and Yiyong Mai*

Cite This: https://dx.doi.org/10.1021/jacs.0c07013

ABSTRACT: Structurally well-defined graphene nanoribbons (GNRs) have emerged as highly promising materials for the next-generation nanoelectronics. The electronic properties of GNRs critically depend on their edge topologies. Here, we demonstrate the efficient synthesis of a curved GNR (**cGNR**) with a combined cove, zigzag, and armchair edge structure, through bottom-up synthesis. The curvature of the **cGNR** is elucidated by the corresponding model compounds tetrabenzo[*a,cd,j,lm*]perylene (**1**) and diphenanthrene-fused tetrabenzo[*a,cd,j,lm*]perylene (**2**), the structures of which are unambiguously confirmed by the X-ray single-crystal analysis. The resultant multi-edged **cGNR** exhibits a well-resolved absorption at the near-infrared (NIR) region with a maximum peak at 850 nm, corresponding to a narrow optical energy gap of ∼1.22 eV. Employing THz spectroscopy, we disclose a long scattering time of ∼60 fs, corresponding to a record intrinsic charge carrier mobility of ∼600 $cm^2 V^{-1} s^{-1}$ for photogenerated charge carriers in **cGNR**.

Atomically precise graphene nanoribbons (GNRs) have attracted significant attention in recent years due to their fascinating electronic properties and potential applications in nanoelectronic devices.[1−6] Both theoretical and experimental studies have demonstrated that the electronic and magnetic properties of GNRs are critically dependent on their widths and edge topologies.[7,8] Therefore, the synthesis of atomically precise GNRs with controlled energy gaps is highly desirable not only for their fundamental physicochemical studies but also for their promising applications in carbon-based nanoelectronics.[9−12] In contrast to armchair-edged GNRs (AGNRs) displaying semiconducting property with a direct energy gap,[13] zigzag-edged GNRs (ZGNRs) typically exhibit narrow bandgaps and localized edge states.[14,15] The structurally defined AGNRs have been successfully synthesized in the past decade,[16−21] while the ZGNRs remained less explored due to the highly unstable zigzag edges. In addition, cove-edged GNRs with unique curved geometry are attractive because they can exhibit improved dispersibility in solution, and provide an additional means to control the optoelectronic properties of GNRs.[7,22,23] Thereby, the combination of armchair, cove, and zigzag edge structures can impart GNRs with unique geometries and physiochemical properties that are not accessible by those with solely one type of edge structures.

Here, we demonstrate the first solution synthesis of a curved GNR (**cGNR**) with a combined cove, zigzag and armchair edge structure, which possesses a width of 0.7 nm and an average length of 23 nm. Two model compounds as the subunits of the **cGNR**, namely tetrabenzo[*a,cd,j,lm*]perylene (**1**) and diphenanthrene-fused tetrabenzo[*a,cd,j,lm*]perylene (**2**) containing a double [4]helicene unit (Scheme 1), are synthesized. Single-crystal structures of **1** and **2**, along with the density functional theory (DFT) simulation clearly elucidate the curvature of the corresponding **cGNR**. The **cGNR** exhibits a well-resolved absorption in the near-infrared (NIR) region with a maximum peak at ∼850 nm. To date, this is the longest wavelength among the reported solution-processable GNRs,[17,21,24−26] corresponding to a quite narrow optical energy gap of 1.22 eV for this **cGNR**, slightly higher than the lowest bandgap of 1.03 eV reported for solution-based GNRs.[21] Employing contact-free terahertz (THz) spectroscopy, we demonstrate that the **cGNR** possesses a record-high intrinsic carrier mobility of up to ∼600 $cm^2 V^{-1} s^{-1}$, making it a promising material for optoelectronic devices.[27] Our study provides a strategy to simultaneously achieve a narrow width, good dispersibility, low bandgap, and high carrier mobility for GNRs by introducing a multi-edge structure.

First, model compounds **1** and **2**, which can be regarded as the short segments of **cGNR**, and monomer 1,8-bis(2-bromophenyl)benzo[*k*]tetraphene (**3**) for the GNR, were synthesized (Scheme 1). Compound 4,4′-((2,5-dibromo-1,4-phenylene)bis(ethyne-2,1-diyl))bis(*tert*-butylbenzene) (**4a**) was synthesized from 1,4-dibromo-2,5-diiodobenzene via Sonogashira coupling in 87% yield (Scheme S1). A Suzuki coupling of **4a** with 2-biphenylboronic acid gave 1,4-bis(2′-biphenyl)-2,5-bis(4-(*tert*-butyl)phenyl)ethynylbenzene (**5a**) in 92% yield. ICl-mediated benzannulation afforded 5,12-bis(4-

Received: July 2, 2020

https://dx.doi.org/10.1021/jacs.0c07013
J. Am. Chem. Soc. XXXX, XXX, XXX−XXX

Scheme 1. Schematic Illustration of the Synthesis of 1, 2, and 3

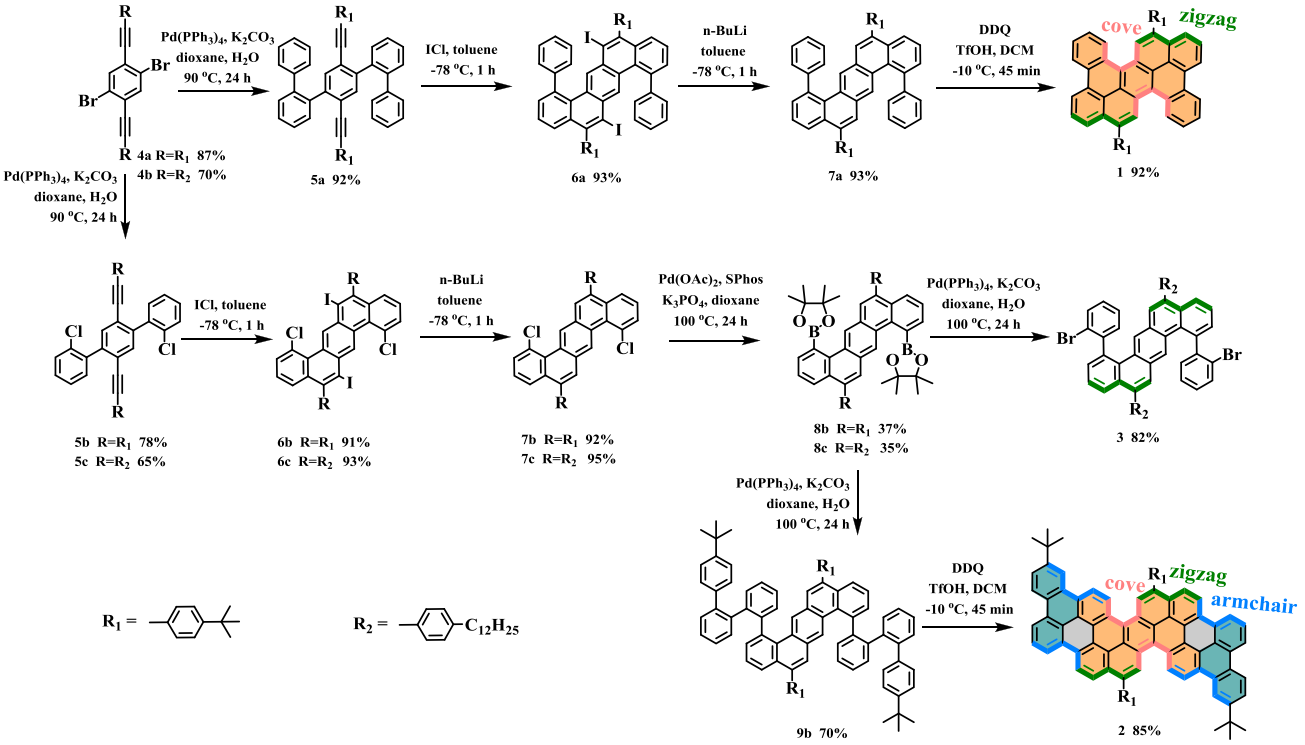

(*tert*-butyl)phenyl)-6,13-diiodo-1,8-diphenylbenzo[*k*]-tetraphene (**6a**) in 93% yield. After the treatment of **6a** with *n*-butyllithium, 5,12-bis(4-(*tert*-butyl)phenyl)-1,8-diphenyl-benzo[*k*]tetraphene (**7a**) was synthesized in 93% yield. Then, compound **1** was achieved through the Scholl reaction of **7a** in 92% yield. Following the similar synthetic strategies, compound **2** and monomer **3** were successfully synthesized with the yields of 82% and 85%, respectively (see details in the Supporting Information (SI)).

The chemical identities of **1** and **2** were confirmed via high-resolution mass spectrometry (HR-MS) (Figure S1) and NMR analysis (Figures S2−S11). Notably, compound **2** exhibits a significant tendency to form aggregates after dissolution in 1,1,2,2-tetrachloroethane-d_2, resulting in a slow increase of ^{1}H NMR signal width. This effect can be reversed by heat treatment and dilution (Figure S11). Besides, the crystals of **1** and **2** were grown by slow evaporation of their solutions in methanol/dichloromethane (DCM) and *n*-hexane/carbon disulfide, respectively, allowing to reveal their structural features by the X-ray single-crystal analysis (Figure 1). Both **1** and **2** adopt perfect centrosymmetric structures, and their (*P*,*P*) and (*M*,*M*) enantiomers present in a ratio of 1:1 in the solid-state. Both **1** and **2** manifest a curved geometry due to the steric repulsion of hydrogen atoms of the double [4]helicene segments (Figure 1). The dihedral angle between plane C1−C2−C3 and plane C3−C4−C5 is 38.7° in **1** (Figure 1a), which is slightly larger than that of **2** (36.5°, Figure 1b) and well comparable with those of the reported double [4]helicenes.[22]

The synthesis of **cGNR** is illustrated in Scheme 2a. First, monomer **3** was synthesized from 1,4-dibromo-2,5-diiodobenzene over eight steps (Scheme 1). Second, the poly(diphenyl benzo[*k*]tetraphene) (**P1**) substituted with dodecylphenyl groups was prepared by the AA-type Yamamoto polymerization of **3** (Scheme 2a). Gel permeation chromatography

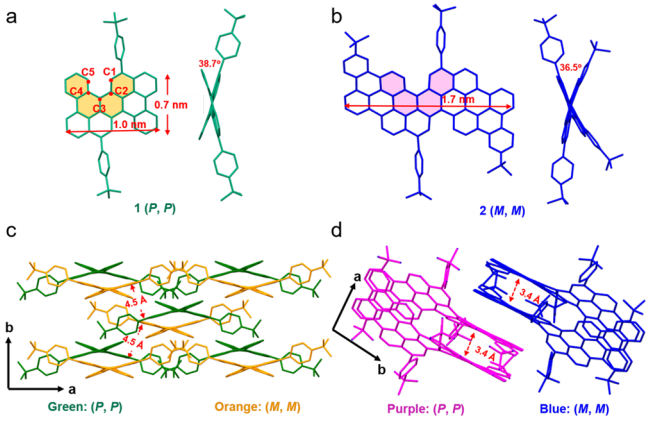

Figure 1. X-ray crystal structures of **1** and **2**. All hydrogen atoms and solvent molecules are omitted for clarity. (a, b) Top and side views of **1** (*P*,*P*) and **2** (*M*,*M*). (c, d) Crystal packing of **1** and **2**.

(GPC) analysis against linear polystyrene standard revealed that the number-average molecular weight (M_n) of the **P1** is around 18 100 g mol^{-1} with a narrow dispersity of 1.15 (Figure S12). The MS spectrum of the resultant **P1** displays that the *m*/*z* intervals are well consistent with the exact mass of repeating unit diphenylbenzo[*k*]tetraphene (917 g mol^{-1}) (Figure S13). Finally, **cGNR** was obtained through the Scholl reaction of **P1** with $FeCl_3$ (7.5 equiv/H) as the Lewis acid and oxidant in DCM for 3 days. The resultant **cGNR** possesses a combined cove, zigzag, and armchair edge structure with a width of 0.7 nm (Scheme 2a). The estimated average length of **cGNR** is about 23 nm based on the M_n of **P1** (Figure S12b).

The successful cyclodehydrogenation of **P1** was first demonstrated by Fourier transform infrared (FTIR) (Figure 2a) and Raman (Figure 2b) investigations. FTIR spectrum of the **cGNR** revealed a significant attenuation of the bands from

https://dx.doi.org/10.1021/jacs.0c07013
J. Am. Chem. Soc. XXXX, XXX, XXX−XXX

Scheme 2. (a) Synthetic Route toward cGNR and (b) the Geometry of cGNR by DFT Simulation

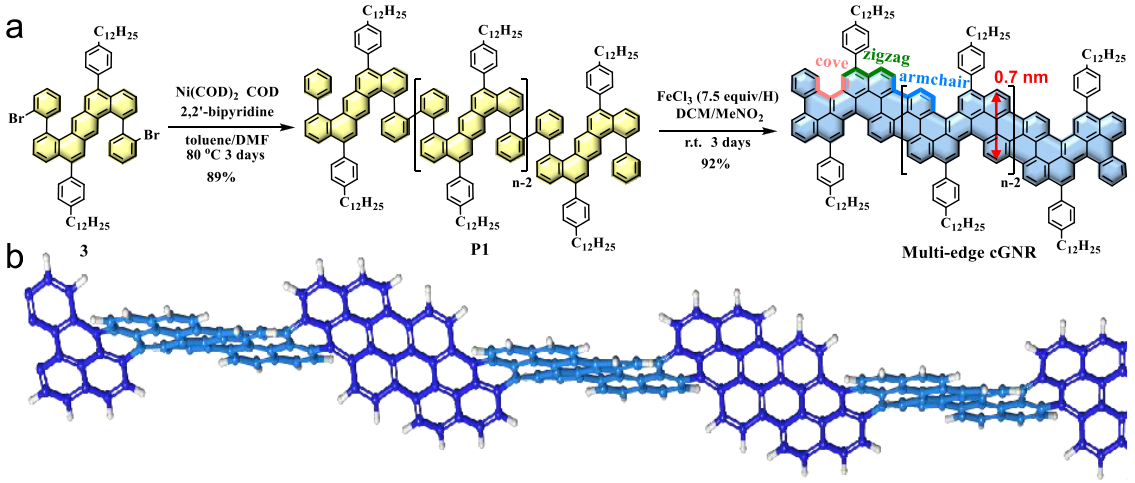

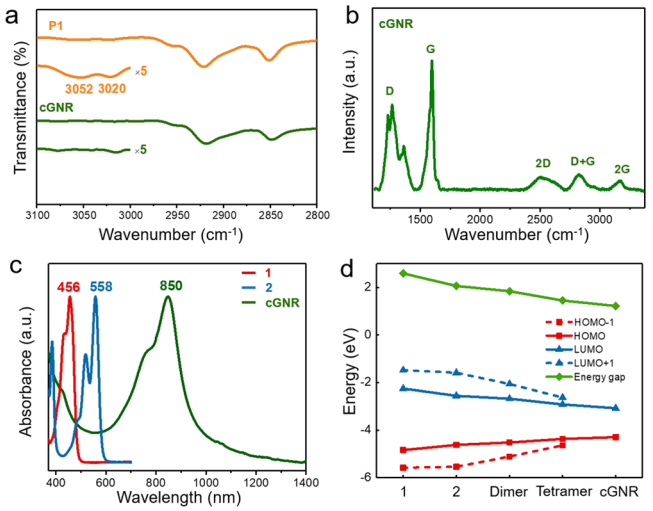

Figure 2. Spectroscopic characterizations of the **cGNR**. (a) FTIR spectra of **P1** and the **cGNR**. (b) Raman spectrum of the **cGNR** measured at 532 nm. (c) UV-vis absorption spectra of the **cGNR** in chloroform (0.1 mg mL^{-1}) and **1**, **2** in DCM (10^{-5} M). (d) Calculated energy level of **1**, **2**, dimer (Figure S22), tetramer (Figure S22), and **cGNR**.

aromatic C−H stretching vibrations at 3052 and 3020 cm^{-1} after the oxidative cyclodehydrogenation, with respect to the spectrum of the **P1**, suggesting the efficient graphitization[28] (Figure 2a). The successful formation of **cGNR** was further confirmed by solid-state NMR measurements (Figures S15 and S16). The comparison of the ^1H NMR magic-angle spinning (MAS) spectra (Figure S15) of **P1** and **cGNR** demonstrated a clear increase in ^1H line width after graphitization. Moreover, the reduced $\pi-\pi$ stacking of the **cGNR** can be identified in the 2D $^1H-^1H$ double-quantum single-quantum (DQ-SQ) NMR correlation spectrum (Figure S15). The $^1H-^1H$ auto-correlation signals of the aromatic protons fall in a much narrower range compared to other structurally similar GNRs.[27] The narrower range of ^1H chemical shifts is a clear indication of reduced $\pi-\pi$ stacking effects in the **cGNR**, which can be attributed to the nonplanar nature of **cGNR**. The Raman spectrum of the **cGNR** exhibits a multi-component D band at 1300 cm^{-1} and G band at 1597 cm^{-1}. Combination and high-order modes are identified at 2506, 2835, and 3169 cm^{-1} (Figure 2b). Clear differences with in-plane GNRs are seen by performing multi-wavelength Raman spectroscopy: first, the D and G bands split into several components when using a laser excitation energy of 1.96 eV, possibly due to resonant effects associated with the unique structure of **cGNR** (Figures S17–S20);[29,30] second, the G peak shows a dispersion of ~27 cm^{-1}/eV (Figure S19b), which is much higher than that reported for in-plane GNRs, possibly deriving from the disruption of the aromatic core of the nonplanar ribbons.

Thanks to the long alkyl chain decoration at the edges and the nonplanar geometry, the **cGNR** can be readily dispersed in common organic solvents, including chloroform, tetrahydrofuran, and toluene, etc. Mild sonication enables the formation of green stable dispersion of the **cGNR** with a high concentration of 0.1 mg mL^{-1} in chloroform. From the UV-vis-NIR absorption spectra of compounds **1** and **2** in DCM (Figure 2c), the energy gap of **2** is inferred to be 2.1 eV, which is lower than that of **1** (2.5 eV). Compared to **1** and **2**, **cGNR** displays a significantly red-shifted absorption to the NIR region with a maximum absorption peak at ~850 nm. The optical energy gap of **cGNR** is calculated to be 1.22 eV, which is quite small compared with those of the reported solution-processable GNRs.[17,21,24−26] DFT simulation confirms the up-down conformation of **cGNR** (Scheme 2b), in line with the crystal structure data of its corresponding model compounds **1** and **2**. In addition, the energy gaps of **1**, **2**, and **cGNR** are calculated to be 2.59, 2.06, and 1.22 eV, respectively, in excellent agreement with the experimental results (Figure 2d).

The excellent solution processability of the **cGNR** in various organic solvents makes it promising for optoelectronic applications. Toward this end, we further investigated the electronic transport properties of **cGNR**, both in dispersion and thin-film geometries (produced by drop cast), using ultrafast terahertz spectroscopy. In the studies, charge carriers are optically injected into **cGNR** by a ~50 fs visible laser pulse, and their complex conductivity is subsequently probed by a single-cycle THz pulse (with ~1 ps duration). Optical-pump THz-probe spectroscopy (OPTP) measures the short-range conductivity, typically within one nanoribbon. Figure 3a illustrates the time-resolved dynamics for both the real and imaginary conductivities for **cGNR** dispersed in 1,2,4-trichlorobenzene. The sub-picosecond rise in the real conductivity indicates the optical injection of free charges into the GNRs following the photoexcitation (with the pump

https://dx.doi.org/10.1021/jacs.0c07013
J. Am. Chem. Soc. XXXX, XXX, XXX−XXX

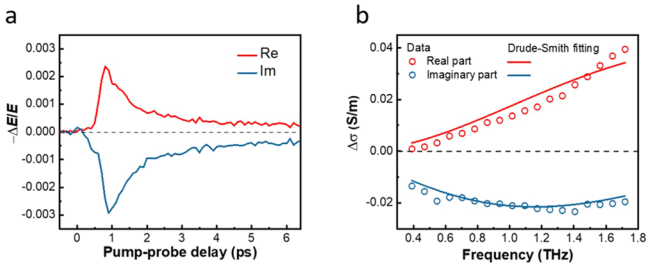

Figure 3. (a) Time-resolved terahertz photoconductivity (proportional to the relative changes in the transmitted field, $-\Delta E/E$) of **cGNR** following photoexcitation. The samples are photoexcited by a short ~50 fs laser pulse with the photon energy of 2.4 eV and an absorbed photon density of 1.8×10^{15} cm^{-2}. (b) The frequency-resolved THz complex conductivity measured at 1.5 ps after photoexcitation. The solid lines represent the Drude−Smith fitting following the discussion in the main text and SI.

photon energy of 2.4 eV). The subsequent rapid decay is consistent with the formation of the bound electron−hole pairs (excitons).[31,32] The frequency-resolved THz photoconductive response at ~1.5 ps after photoexcitation is shown in Figure 3b. The data can be well accounted for by the Drude−Smith model (see SI), which describes the transport of free charges subject to backscattering due to, e.g., structural deformations.[24,33−35] In the model, a parameter c characterizes the backscattering probability, ranging between 0 (random backscattering) to −1 (preferential backscattering). The best fit to the data yields $c = -1 \pm 0.02$. The preferential backscattering presumably occurs at the ends of the **cGNR**. Remarkably, the charge scattering time τ is found to be 57 ± 3 fs, substantially larger than those of previously studied GNRs with the armchair edge (20−30 fs).[34,36] Using $\mu = e\tau / m^*$, with m^* the effective mass (obtained by DFT calculations, see SI), we infer a record intrinsic carrier mobility μ of 617 ± 32 $cm^2 V^{-1} s^{-1}$. Finally, we compare the transport properties of GNRs in dispersion to that in the thin film (by drop cast). As shown in Figure S25, we obtain the same charge scattering τ of 58 ± 3 fs, and a c parameter of ~ −0.96. Therefore, our THz study not only reveals a high intrinsic mobility of charge carriers in **cGNR**, but also demonstrates that the deposition of the **cGNR** into a solid film does not introduce additional charge scattering events. On the other hand, the inferred c parameters indicate a full confinement of the charge carriers for the ribbon dispersed in solution (with $1 + c = 0$), and some degree of charge delocalization between ribbons on the substrates thanks to the inter-ribbon coupling (with $1 + c > 0$, see SI for details).

In summary, we demonstrated the bottom-up solution synthesis of a novel **cGNR** with combined edge structures of cove, zigzag, and armchair. Model compounds **1** and **2** were also synthesized to manifest the double [4]helicene structures, resulting in a curved geometry of the corresponding **cGNR**. The **cGNR** exhibited excellent liquid-phase dispersibility and unprecedented absorption in the NIR region, with a maximum peak at ~850 nm and a particularly narrow optical energy gap of ~1.22 eV. THz studies revealed equally high charge scattering time (~60 fs) and a record high intrinsic charge carrier mobility of ~600 $cm^2 V^{-1} s^{-1}$ for GNRs. The GNRs with multi-edge structure hold great promise in many applications, including photothermal conversion, photovoltaics, and nanoelectronic devices.

■ ASSOCIATED CONTENT

Supporting Information

The Supporting Information is available free of charge at https://pubs.acs.org/doi/10.1021/jacs.0c07013.

Experimental details; supporting Schemes S1 and S2, Figures S1−S63, and Tables S1−S3; and calculations of the model compounds and **cGNR** (PDF)

X-ray crystallographic data for **1** (CIF)

X-ray crystallographic data for **2** (CIF)

■ AUTHOR INFORMATION

Corresponding Authors

Junzhi Liu − *Center for Advancing Electronics Dresden (cfaed), Faculty of Chemistry and Food Chemistry, Technische Universität Dresden, D-01062 Dresden, Germany; Department of Chemistry and State Key Laboratory of Synthetic Chemistry, The University of Hong Kong, Hong Kong 999077, China;* orcid.org/0000-0001-7146-0942; Email: juliu@hku.hk

Yiyong Mai − *School of Chemistry and Chemical Engineering, Frontiers Science Center for Transformative Molecules, Shanghai Key Laboratory of Electrical Insulation and Thermal Ageing, Shanghai Jiao Tong University, Shanghai 200240, China;* orcid.org/0000-0002-6373-2597; Email: mai@sjtu.edu.cn

Authors

Wenhui Niu − *School of Chemistry and Chemical Engineering, Frontiers Science Center for Transformative Molecules, Shanghai Key Laboratory of Electrical Insulation and Thermal Ageing, Shanghai Jiao Tong University, Shanghai 200240, China; Center for Advancing Electronics Dresden (cfaed), Faculty of Chemistry and Food Chemistry, Technische Universität Dresden, D-01062 Dresden, Germany*

Ji Ma − *Center for Advancing Electronics Dresden (cfaed), Faculty of Chemistry and Food Chemistry, Technische Universität Dresden, D-01062 Dresden, Germany;* orcid.org/0000-0003-4418-2339

Paniz Soltani − *Max Planck Institute for Polymer Research, D-55128 Mainz, Germany*

Wenhao Zheng − *Max Planck Institute for Polymer Research, D-55128 Mainz, Germany*

Fupin Liu − *Leibniz Institute for Solid State and Materials Research, D-01069 Dresden, Germany;* orcid.org/0000-0002-8454-726X

Alexey A. Popov − *Leibniz Institute for Solid State and Materials Research, D-01069 Dresden, Germany;* orcid.org/0000-0002-7596-0378

Jan J. Weigand − *Department of Inorganic Molecular Chemistry, Technische Universität Dresden, D-01062 Dresden, Germany;* orcid.org/0000-0001-7323-7816

Hartmut Komber − *Leibniz-Institut für Polymerforschung Dresden e.V., D-01069 Dresden, Germany;* orcid.org/0000-0001-6176-6737

Emanuele Poliani − *Department of Chemistry, Manchester University, Manchester M13 9PL, United Kingdom;* orcid.org/0000-0003-1802-4775

Cinzia Casiraghi − *Department of Chemistry, Manchester University, Manchester M13 9PL, United Kingdom;* orcid.org/0000-0001-7185-0377

Jörn Droste − *Institute of Physical Chemistry, Westfälische Wilhelms-Universität (WWU) Münster, D-48149 Münster, Germany*

https://dx.doi.org/10.1021/jacs.0c07013
J. Am. Chem. Soc. XXXX, XXX, XXX−XXX

Michael Ryan Hansen − *Institute of Physical Chemistry, Westfälische Wilhelms-Universität (WWU) Münster, D-48149 Münster, Germany;* orcid.org/0000-0001-7114-8051
Silvio Osella − *Biological Systems Simulation Lab, Center of New Technologies, University of Warsaw, 02-097 Warsaw, Poland;* orcid.org/0000-0001-8541-1914
David Beljonne − *Laboratory for Chemistry of Novel Materials, Université de Mons, B-7000 Mons, Belgium;* orcid.org/0000-0002-2989-3557
Mischa Bonn − *Max Planck Institute for Polymer Research, D-55128 Mainz, Germany;* orcid.org/0000-0001-6851-8453
Hai I. Wang − *Max Planck Institute for Polymer Research, D-55128 Mainz, Germany;* orcid.org/0000-0003-0940-3984
Xinliang Feng − *Center for Advancing Electronics Dresden (cfaed), Faculty of Chemistry and Food Chemistry, Technische Universität Dresden, D-01062 Dresden, Germany;* orcid.org/0000-0003-3885-2703

Complete contact information is available at: https://pubs.acs.org/10.1021/jacs.0c07013

Funding

Y.M. is grateful for financial support from the National Natural Science Foundation of China (21774076 and 52073173) and Program of Shanghai Academic Research Leader (19XD1421700). J.D. thanks the Deutsche Forschungsgemeinschaft (DFG) for funding (SFB 858). X.F. thanks the European Union's Horizon 2020 (No. 881603 Graphene Flagship Core3, No. 813036 Marie Skłodowska-Curie), ERC Grant T2DCP, German DFG (Cluster of Excellence "Center for Advancing Electronics Dresden (cfaed)", and EnhanceNano (No. 391979941) as well as the European Social Fund and the Federal State of Saxony (ESFProject "GRAPHD", TU Dresden). J.L. is grateful for startup funding from The University of Hong Kong and funding support from ITC to the SKL. C.C. thanks the European Commission in the framework of ERC Grant NOC2D.

Notes

The authors declare no competing financial interest.
[¶]P.S.: deceased, January 8, 2020.

■ ACKNOWLEDGMENTS

We are grateful for the assistance of Mr. Enrique Caldera Cruz from Leibniz Institute for Polymer Research Dresden for the GPC measurements. We thank F. Drescher and Prof. E. Brunner for HR-MS measurements. Diffraction data were collected on BL14.3 at the BESSY II electron-storage ring operated by Helmholtz-Zentrum Berlin; we would particularly like to acknowledge the help and support of Manfred Weiss and his group members during the experiments at BESSY II. We also appreciate the Instrumental Analysis Center at Shanghai Jiao Tong University for some analyses. S.O. thanks the Interdisciplinary Center for Mathematical and Computational Modelling (ICM, University of Warsaw) under the G53-8 and GB80-24 computational grants.

■ REFERENCES

(1) Narita, A.; Wang, X.-Y.; Feng, X.; Müllen, K. New advances in nanographene chemistry. *Chem. Soc. Rev.* **2015**, *44*, 6616−6643.
(2) Yazyev, O. V. A Guide to the Design of Electronic Properties of Graphene Nanoribbons. *Acc. Chem. Res.* **2013**, *46*, 2319−2328.
(3) Segawa, Y.; Ito, H.; Itami, K. Structurally uniform and atomically precise carbon nanostructures. *Nat. Rev. Mater.* **2016**, *1*, 15002.
(4) Huang, Y.; Dou, W.-T.; Xu, F.; Ru, H.-B.; Gong, Q.; Wu, D.; Yan, D.; Tian, H.; He, X.-P.; Mai, Y.; Feng, X. Supramolecular Nanostructures of Structurally Defined Graphene Nanoribbons in the Aqueous Phase. *Angew. Chem., Int. Ed.* **2018**, *57*, 3366−3371.
(5) Niu, W.; Liu, J.; Mai, Y.; Müllen, K.; Feng, X. Synthetic Engineering of Graphene Nanoribbons with Excellent Liquid-Phase Processability. *Trends Chem.* **2019**, *1*, 549−558.
(6) Jolly, A.; Miao, D.; Daigle, M.; Morin, J.-F. Emerging Bottom-Up Strategies for the Synthesis of Graphene Nanoribbons and Related Structures. *Angew. Chem., Int. Ed.* **2020**, *59*, 4624−4633.
(7) Hu, Y.; Xie, P.; De Corato, M.; Ruini, A.; Zhao, S.; Meggendorfer, F.; Straasø, L. A.; Rondin, L.; Simon, P.; Li, J.; Finley, J. J.; Hansen, M. R.; Lauret, J.-S.; Molinari, E.; Feng, X.; Barth, J. V.; Palma, C.-A.; Prezzi, D.; Müllen, K.; Narita, A. Bandgap Engineering of Graphene Nanoribbons by Control over Structural Distortion. *J. Am. Chem. Soc.* **2018**, *140*, 7803−7809.
(8) Chen, L.; Hernandez, Y.; Feng, X.; Müllen, K. From Nanographene and Graphene Nanoribbons to Graphene Sheets: Chemical Synthesis. *Angew. Chem., Int. Ed.* **2012**, *51*, 7640−7654.
(9) El Abbassi, M.; Perrin, M. L.; Barin, G. B.; Sangtarash, S.; Overbeck, J.; Braun, O.; Lambert, C. J.; Sun, Q.; Prechtl, T.; Narita, A.; Müllen, K.; Ruffieux, P.; Sadeghi, H.; Fasel, R.; Calame, M. Controlled Quantum Dot Formation in Atomically Engineered Graphene Nanoribbon Field-Effect Transistors. *ACS Nano* **2020**, *14*, 5754−5762.
(10) Mehdi Pour, M.; Lashkov, A.; Radocea, A.; Liu, X.; Sun, T.; Lipatov, A.; Korlacki, R. A.; Shekhirev, M.; Aluru, N. R.; Lyding, J. W.; Sysoev, V.; Sinitskii, A. Laterally extended atomically precise graphene nanoribbons with improved electrical conductivity for efficient gas sensing. *Nat. Commun.* **2017**, *8*, 820.
(11) Llinas, J. P.; Fairbrother, A.; Borin Barin, G.; Shi, W.; Lee, K.; Wu, S.; Yong Choi, B.; Braganza, R.; Lear, J.; Kau, N.; Choi, W.; Chen, C.; Pedramrazi, Z.; Dumslaff, T.; Narita, A.; Feng, X.; Müllen, K.; Fischer, F.; Zettl, A.; Ruffieux, P.; Yablonovitch, E.; Crommie, M.; Fasel, R.; Bokor, J. Short-channel field-effect transistors with 9-atom and 13-atom wide graphene nanoribbons. *Nat. Commun.* **2017**, *8*, 633.
(12) Gao, J.; Uribe-Romo, F. J.; Saathoff, J. D.; Arslan, H.; Crick, C. R.; Hein, S. J.; Itin, B.; Clancy, P.; Dichtel, W. R.; Loo, Y.-L. Ambipolar Transport in Solution-Synthesized Graphene Nanoribbons. *ACS Nano* **2016**, *10*, 4847−4856.
(13) Raza, H.; Kan, E. C. Armchair graphene nanoribbons: Electronic structure and electric-field modulation. *Phys. Rev. B: Condens. Matter Mater. Phys.* **2008**, *77*, 245434.
(14) Ruffieux, P.; Wang, S.; Yang, B.; Sánchez-Sánchez, C.; Liu, J.; Dienel, T.; Talirz, L.; Shinde, P.; Pignedoli, C. A.; Passerone, D.; Dumslaff, T.; Feng, X.; Müllen, K.; Fasel, R. On-surface synthesis of graphene nanoribbons with zigzag edge topology. *Nature* **2016**, *531*, 489−492.
(15) Kan, E.-j.; Li, Z.; Yang, J.; Hou, J. G. Half-Metallicity in Edge-Modified Zigzag Graphene Nanoribbons. *J. Am. Chem. Soc.* **2008**, *130*, 4224−4225.
(16) Yang, X.; Dou, X.; Rouhanipour, A.; Zhi, L.; Räder, H. J.; Müllen, K. Two-Dimensional Graphene Nanoribbons. *J. Am. Chem. Soc.* **2008**, *130*, 4216−4217.
(17) Li, G.; Yoon, K.-Y.; Zhong, X.; Wang, J.; Zhang, R.; Guest, J. R.; Wen, J.; Zhu, X. Y.; Dong, G. A modular synthetic approach for band-gap engineering of armchair graphene nanoribbons. *Nat. Commun.* **2018**, *9*, 1687.
(18) Yang, W.; Lucotti, A.; Tommasini, M.; Chalifoux, W. A. Bottom-Up Synthesis of Soluble and Narrow Graphene Nanoribbons Using Alkyne Benzannulations. *J. Am. Chem. Soc.* **2016**, *138*, 9137−9144.
(19) Li, G.; Yoon, K.-Y.; Zhong, X.; Zhu, X.; Dong, G. Efficient Bottom-Up Preparation of Graphene Nanoribbons by Mild Suzuki−Miyaura Polymerization of Simple Triaryl Monomers. *Chem. - Eur. J.* **2016**, *22*, 9116−9120.
(20) Vo, T. H.; Shekhirev, M.; Kunkel, D. A.; Morton, M. D.; Berglund, E.; Kong, L.; Wilson, P. M.; Dowben, P. A.; Enders, A.;

Sinitskii, A. Large-scale solution synthesis of narrow graphene nanoribbons. *Nat. Commun.* **2014**, *5*, 3189.
(21) Yang, W.; Lucotti, A.; Tommasini, M.; Chalifoux, W. A. Bottom-Up Synthesis of Soluble and Narrow Graphene Nanoribbons Using Alkyne Benzannulations. *J. Am. Chem. Soc.* **2016**, *138*, 9137−9144.
(22) Liu, J.; Li, B.-W.; Tan, Y.-Z.; Giannakopoulos, A.; Sanchez-Sanchez, C.; Beljonne, D.; Ruffieux, P.; Fasel, R.; Feng, X.; Müllen, K. Toward Cove-Edged Low Band Gap Graphene Nanoribbons. *J. Am. Chem. Soc.* **2015**, *137*, 6097−6103.
(23) Yano, Y.; Wang, F.; Mitoma, N.; Miyauchi, Y.; Ito, H.; Itami, K. Step-Growth Annulative π-Extension Polymerization for Synthesis of Cove-Type Graphene Nanoribbons. *J. Am. Chem. Soc.* **2020**, *142*, 1686−1691.
(24) Huang, Y.; Xu, F.; Ganzer, L.; Camargo, F. V. A.; Nagahara, T.; Teyssandier, J.; Van Gorp, H.; Basse, K.; Straasø, L. A.; Nagyte, V.; Casiraghi, C.; Hansen, M. R.; De Feyter, S.; Yan, D.; Müllen, K.; Feng, X.; Cerullo, G.; Mai, Y. Intrinsic Properties of Single Graphene Nanoribbons in Solution: Synthetic and Spectroscopic Studies. *J. Am. Chem. Soc.* **2018**, *140*, 10416−10420.
(25) Huang, Y.; Mai, Y.; Beser, U.; Teyssandier, J.; Velpula, G.; van Gorp, H.; Straasø, L. A.; Hansen, M. R.; Rizzo, D.; Casiraghi, C.; Yang, R.; Zhang, G.; Wu, D.; Zhang, F.; Yan, D.; De Feyter, S.; Müllen, K.; Feng, X. Poly(ethylene oxide) Functionalized Graphene Nanoribbons with Excellent Solution Processability. *J. Am. Chem. Soc.* **2016**, *138*, 10136−10139.
(26) Daigle, M.; Miao, D.; Lucotti, A.; Tommasini, M.; Morin, J.-F. Helically Coiled Graphene Nanoribbons. *Angew. Chem., Int. Ed.* **2017**, *56*, 6213−6217.
(27) Narita, A.; Feng, X.; Hernandez, Y.; Jensen, S. A.; Bonn, M.; Yang, H.; Verzhbitskiy, I. A.; Casiraghi, C.; Hansen, M. R.; Koch, A. H. R.; Fytas, G.; Ivasenko, O.; Li, B.; Mali, K. S.; Balandina, T.; Mahesh, S.; De Feyter, S.; Müllen, K. Synthesis of structurally well-defined and liquid-phase-processable graphene nanoribbons. *Nat. Chem.* **2014**, *6*, 126−132.
(28) Narita, A.; Verzhbitskiy, I. A.; Frederickx, W.; Mali, K. S.; Jensen, S. A.; Hansen, M. R.; Bonn, M.; De Feyter, S.; Casiraghi, C.; Feng, X.; Müllen, K. Bottom-Up Synthesis of Liquid-Phase-Processable Graphene Nanoribbons with Near-Infrared Absorption. *ACS Nano* **2014**, *8*, 11622−11630.
(29) Rizzo, D.; Prezzi, D.; Ruini, A.; Nagyte, V.; Keerthi, A.; Narita, A.; Beser, U.; Xu, F.; Mai, Y.; Feng, X.; Müllen, K.; Molinari, E.; Casiraghi, C. Multiwavelength Raman spectroscopy of ultranarrow nanoribbons made by solution-mediated bottom-up approach. *Phys. Rev. B: Condens. Matter Mater. Phys.* **2019**, *100*, 045406.
(30) Verzhbitskiy, I. A.; Corato, M. D.; Ruini, A.; Molinari, E.; Narita, A.; Hu, Y.; Schwab, M. G.; Bruna, M.; Yoon, D.; Milana, S.; Feng, X.; Müllen, K.; Ferrari, A. C.; Casiraghi, C.; Prezzi, D. Raman Fingerprints of Atomically Precise Graphene Nanoribbons. *Nano Lett.* **2016**, *16*, 3442−3447.
(31) Tries, A.; Osella, S.; Zhang, P.; Xu, F.; Ramanan, C.; Kläui, M.; Mai, Y.; Beljonne, D.; Wang, H. I. Experimental Observation of Strong Exciton Effects in Graphene Nanoribbons. *Nano Lett.* **2020**, *20*, 2993−3002.
(32) Xu, F.; Yu, C.; Tries, A.; Zhang, H.; Kläui, M.; Basse, K.; Hansen, M. R.; Bilbao, N.; Bonn, M.; Wang, H. I.; Mai, Y. Tunable Superstructures of Dendronized Graphene Nanoribbons in Liquid Phase. *J. Am. Chem. Soc.* **2019**, *141*, 10972−10977.
(33) Chen, Z.; Wang, H. I.; Bilbao, N.; Teyssandier, J.; Prechtl, T.; Cavani, N.; Tries, A.; Biagi, R.; De Renzi, V.; Feng, X.; Kläui, M.; De Feyter, S.; Bonn, M.; Narita, A.; Müllen, K. Lateral Fusion of Chemical Vapor Deposited N = 5 Armchair Graphene Nanoribbons. *J. Am. Chem. Soc.* **2017**, *139*, 9483−9486.
(34) Chen, Z.; Wang, H. I.; Teyssandier, J.; Mali, K. S.; Dumslaff, T.; Ivanov, I.; Zhang, W.; Ruffieux, P.; Fasel, R.; Räder, H. J.; Turchinovich, D.; De Feyter, S.; Feng, X.; Kläui, M.; Narita, A.; Bonn, M.; Müllen, K. Chemical Vapor Deposition Synthesis and Terahertz Photoconductivity of Low-Band-Gap N = 9 Armchair Graphene Nanoribbons. *J. Am. Chem. Soc.* **2017**, *139*, 3635−3638.
(35) Ulbricht, R.; Hendry, E.; Shan, J.; Heinz, T. F.; Bonn, M. Carrier dynamics in semiconductors studied with time-resolved terahertz spectroscopy. *Rev. Mod. Phys.* **2011**, *83*, 543−586.
(36) Ivanov, I.; Hu, Y.; Osella, S.; Beser, U.; Wang, H. I.; Beljonne, D.; Narita, A.; Müllen, K.; Turchinovich, D.; Bonn, M. Role of Edge Engineering in Photoconductivity of Graphene Nanoribbons. *J. Am. Chem. Soc.* **2017**, *139*, 7982−7988.

https://dx.doi.org/10.1021/jacs.0c07013
J. Am. Chem. Soc. XXXX, XXX, XXX−XXX